Nanoscale

Lipid composition dictates serum stability of reconstituted high-density lipoproteins: implications for in vivo applications

Journal:	*Nanoscale*
Manuscript ID	NR-ART-12-2017-009690.R1
Article Type:	Paper
Date Submitted by the Author:	16-Feb-2018
Complete List of Authors:	Gilmore, Sean; Lawrence Livermore National Laboratory, Carpenter, Timothy; Lawrence Livermore National Laboratory Ingolfsson, Helgi; Lawrence Livermore National Laboratory Peters, Sandra; Lawrence Livermore National Laboratory Henderson, Pual; University of California Davis Department of Internal Medicine Blanchette, Craig; Lawrence Livermore National Laboratory Fischer, Nicholas; Lawrence Livermore National Lab,

Lipid composition dictates serum stability of reconstituted high-density lipoproteins: implications for in vivo applications

Sean F. Gilmore,[1] Timothy S. Carpenter,[1] Helgi I. Ingólfsson,[1] Sandra K. G. Peters,[1] Paul T. Henderson,[2] Craig D. Blanchette,[1] Nicholas O. Fischer[1*]

[1] Lawrence Livermore National Laboratory, Livermore, CA, 94550

[2] University of California—Davis (UC Davis) and UC Davis Comprehensive Cancer Center, Sacramento, California 95817

*fischer29@llnl.gov

Abstract

Nanolipoprotein particles (NLPs) are reconstituted high-density lipoproteins, consisting of a phospholipid bilayer stabilized by an apolipoprotein scaffold protein. This class of nanoparticle has been a vital tool in the study of membrane proteins, and in recent years has been increasingly used for *in vivo* applications. Previous work demonstrated that the composition of the lipid bilayer component affects the stability of these particles in serum solutions. In the current study, NLPs assembled with phosphatidylcholine lipids featuring different acyl chain structures were systematically tested to understand the effect that lipid composition has on NLP stability in both neat serum and cell culture media supplemented with 10% serum by volume. The time at which 50% of the particles dissociate, as well as the fraction of the initial population that remains resistant to dissociation, were correlated to key parameters obtained from all-atom simulations of the corresponding lipid bilayers. A significant correlation was observed between the compressibility modulus of the lipid bilayer and particle stability in these complex biological milieu. These results can be used as a reference in preparing particles with tunable stability for *in vitro* and *in vivo* applications of these versatile biological nanoparticles.

Introduction

Nanolipoprotein particles (NLPs) and other types of reconstituted high-density lipoproteins (rHDLs) are gaining significant attention as a vehicle capable of delivering cargo for *in vitro* or *in vivo* applications.[1–3] Like their biological counterparts, these nanoparticles are comprised of a lipid bilayer disc (8-25 nm in diameter) that is stabilized by apolipoproteins[4–6] or truncated mimetics such as amphipathic peptides.[7–9] These particles are extremely versatile in that many different lipids or lipophilic constituents can be incorporated into the lipid bilayer, either comprising a minor component or the bulk of the particle bilayer.[2] The ability to tailor the bilayer and functional elements associated with the bilayer facilitates the use of rHDLs for a wide variety of applications, ranging from structure and function studies of membrane proteins[10] to formulating vaccines for *in vivo* use.[11–14] A defining feature of rHDLs is the "soft" nature of this nanoparticle. In contrast to other nanoparticle systems, rHDLs are held together with weaker, non-covalent forces between the lipid and protein constituents. rHDLs prepared with 1,2-dioleoyl-*sn*-glycero-3-phosphocholine (DOPC) and 1,2-dimyristoyl-*sn*-glycero-3-phosphocholine (DMPC), two of the most commonly used lipids in preparing this class of particle, were shown to be highly susceptible to environmental conditions, which readily disrupted the weak intermolecular interactions necessary for rHDL integrity, ultimately leading to particle dissociation.[15] A number of parameters greatly influence the stability of rHDLs, including lipid bilayer constituents such as cholesterol and lipid headgroup.[16,17] In another defining study, the thermal stability of rHDLs was shown to correlate with acyl chain length of the bilayer lipids, whereby rHDLs prepared with lipids featuring longer acyl chains provided greater resistance to thermally-induced dissociation.[18]

Particle stability has direct relevance to the utility of rHDLs for *in vivo* delivery applications. Particle dissociation and remodeling *in vivo* can lead to the premature release of cargo molecules associated with the rHDL. This is particularly disadvantageous if targeting moieties are employed to direct *in vivo* localization, as particle will decouple the targeting molecules from the cargo molecules, effectively precluding targeted delivery. As such, a key stability parameter to understand is the rate at which the engineered rHDL particle begins to dissociate in physiologically-relevant milieu, as any disruption in the original composition can lead to decoupling of the targeting and cargo moieties. Although several studies have demonstrated that

synthetic HDLs persist *in vivo* for hours, these studies tracked a single constituent[19–21], rather than the overall integrity of the original particle. Our previous work demonstrated that DOPC NLPs rapidly dissociate while circulating[22], demonstrating the need to more thoroughly characterize *in vivo* particle stability as a function of the intact (as-prepared) particle, rather than a single constituent.

To begin a systematic evaluation of NLP stability *in vivo*, this study examines the role of lipid acyl chain structure on the stability of NLPs in experimentally and physiologically relevant media. While others have studied the effects of acyl chain structure on particle stability,[18] relatively few studies have compared how different lipid species affect the particle stability in conditions simulating cell culture or *in vivo* conditions.[15,22] While those studies highlighted the differential stability in these conditions of the particles prepared with different lipids,[15] a thorough understanding of the contribution of lipid features such as chain length and degree of saturation to particle stability is unexplored. To extend our knowledge of particle stability, as well as the fate of these particles once exposed to serum, we have performed systematic stability tests with particles formulated with a range of homogeneous lipid compositions. These tests assessed the separation of the NLP scaffold protein from the lipid bilayer as a measure of degradation from the particle's original, as-prepared structure, although some remanents of the bilayer structure may still be intact (likely associated with endogenous proteins).[8] To mimic relevant biological environments, NLP stability was assessed at 37°C both in undiluted (neat) fetal bovine serum and cell culture media supplemented with 10% serum. To decouple potential differences in headgroup composition and polarity, only phosphatidylcholine lipids were studied to focus primarily on the effect of lipid acyl chain length and saturation (i.e. the number and orientation of double bonds) on particle stability. To correlate stability with lipid composition, molecular dynamics (MD) simulations were used to calculate key intrinsic properties for the different lipid bilayer types used in the study. Our results demonstrate that NLP stability correlates directly with the area expansion modulus, K_A, which is dictated by acyl chain length and saturation. These findings provide key insight into NLP stability and establish a basis for optimizing NLP formulations for specific biological applications.

Results and Discussion

Lipid acyl chain structure modulates NLP stability in cell media with 10% FBS

All NLPs in these studies were fluorescently labeled to analyze particle integrity by size exclusion chromatography (SEC) using an in-line fluorescence detector. NLPs were prepared with the N-terminal 22 kDa fragment of human apoE4 as previously described with exceptions as noted in the methods section (Fig. 1a). Alexa Fluor 488 was used to label the NLP scaffold proteins, and example fluorescence chromatograms of these formulations in PBS are shown in Fig. S1.

RPMI-1640 cell culture media (supplemented with 10% fetal bovine serum and 0.1% antibiotics) was chosen as a representative cell culture media formulation. NLPs were diluted in media, incubated at 37°C, and analyzed by analytical SEC (aSEC) using a Superdex 200 Increase 3.2/300 column (0.2mL/min flow rate) to enable separation and discrimination between the intact particles and the free scaffold protein (eluting at 6-8 or 9-10 minutes, respectively). The fluorescence chromatogram was then analyzed to calculate NLP peak areas, which decrease over time in serum solutions (Fig. 1b, full chromatograms in Fig. S2). Integrated peak areas were fitted to a curve to analyze the change in measured NLP peak area over time. Additionally, 95% confidence bands were calculated for these curves, typically following a one-phase, exponential decay curve (unless noted otherwise). These data were used to calculate the time at which 50% of the initial NLP peak area remained (denoted herein as $t_{1/2}$).

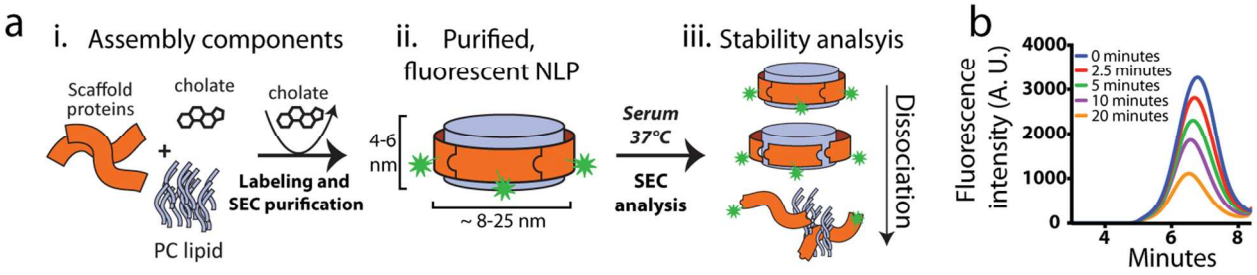

Fig. 1. (a) Schematic of NLP assembly and stability assessment. Purified apolipoproteins were added to cholate-solubilized lipids in PBS (i). Self-assembled NLPs were labeled with NHS-actived Alexa Flour 488 and purified by aaSEC (ii). Fluorescent NLPs were then incubated in serum or media, and periodically assessed by aSEC to monitor NLP dissociation using fluorescence (iii). (b) SEC traces of fluorescently-labeled 22:1 NLPs incubated in neat serum at 37°C for different lengths of time.

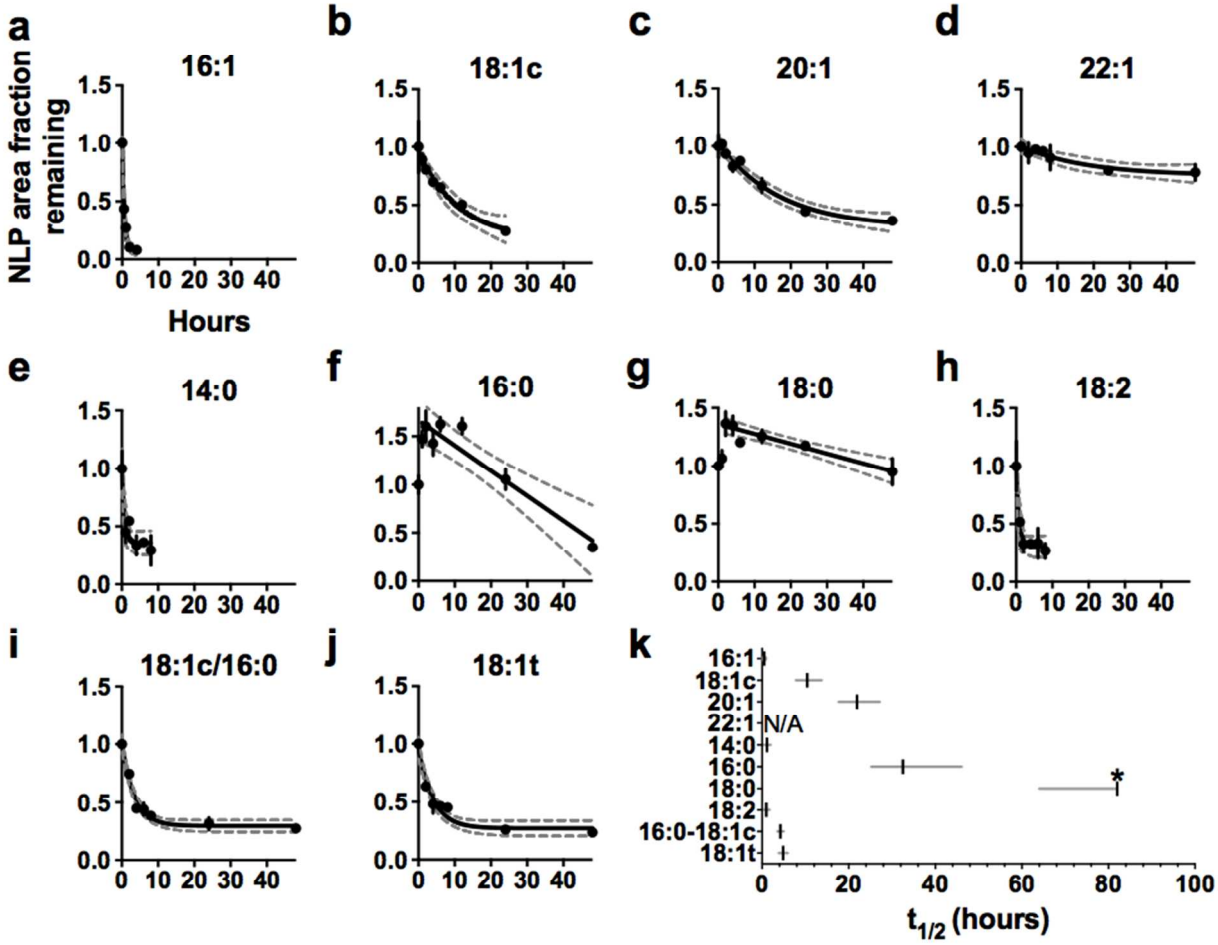

Fig. 2. Charaterization of NLP stability in media supplemented with 10% serum, measuring the change in NLP peak area fraction over time at 37°C. (a-j) Individual stability assessments, whereby X- and Y-axes are represented as the NLP area fraction remaining relative to t=0 and incubation time in hours, respectively. The coefficient of determination (R^2) is listed for each fitted regression fit. (a) 16:1 NLP, $R^2 = 0.99$. (b) 18:1 NLP, $R^2 = 0.91$. (c) 20:1 NLP, $R^2 = 0.96$. (d) 22:1 NLP, $R^2 = 0.73$. (e) 14:0 NLP, $R^2 = 0.84$. (f) 16:0 NLP, $R^2 = 0.90$. (g) 18:0 NLP, $R^2 = 0.82$. (h) 18:2 NLP, $R^2 = 0.90$. (i) 16:0-18:1 cis NLP, $R^2 = 0.93$. (j) 18:1 trans NLP, $R^2 = 0.95$. (k) Summary graph of $t_{1/2}$ values, asterisk indicates an extrapolated value. ND indicates 'not determined'.

To assess the effects of lipid acyl chain length and saturation on stability, NLPs were prepared with homogeneous bilayers consisting of lipids featuring mono-unsaturated acyl chains (16 – 22 carbons), saturated acyl chains (14 – 18 carbons), and one lipid with poly-unsaturated chains. The measured NLP $t_{1/2}$ values in supplemented media increase concomitantly with acyl chain length (Fig. 2). NLPs prepared with a homogeneous 16:1 bilayer dissociated within 1 hour (Fig.

2a), whereas 18:1 and 20:1 NLPs were increasingly stable up to 24 hours (Fig. 2b and 2c). NLPs featuring a 22:1 bilayer were stable beyond 48 hours (Fig. 2d). The 22:1 NLPs exhibit only a minimal loss of NLP area over a 48-hour incubation period, plateauing with approximately 75% of NLPs remaining intact. As such, a $t_{1/2}$ for this formulation could not be experimentally determined under these conditions. All $t_{1/2}$ values and 95% confidence bands are summarized in Table 1.

Similar stability profiles were observed with NLPs prepared with homogeneous bilayers of lipids with saturated chains (14:0 through 18:0). The 14:0 NLPs dissociated rapidly in under 1 hour (Fig. 2e), which is consistent with previous results.[15] A one-phase decay curve could not be fit to the 16:0 (Fig. 2f) or 18:0 (Fig. 2g) NLP data, so rather a linear fit was used. Interestingly, for both of these formulations, the NLP peak area increased to approximately 150% of the initial area after 1 hour. To take these changes into consideration, the t = 0 timepoint was excluded for the fit for the 16:0 series, and the t = 0 and 1 hr timepoints were excluded for the 18:0 series. Further, the y intercept of the fit curve was taken as the initial NLP area value to compute the $t_{1/2}$. For 16:0 NLPs, the NLP peak area value remained relatively steady for the first 12 hours of measurement, but measurements at 24 and 48 hours did decrease below the initial value. For this formulation, we calculated a $t_{1/2}$ of approximately 33 hours. While the peak area for 16:0 NLPs did decrease below the initial value, this was not the case for the 18:0 NLPs, although a gradual area decrease was observed during the 48 hour measurement period. This data was used to calculate a $t_{1/2}$ of 82 hours for the 18:0 NLPs with a lower boundary of 64 hours for the 95% confidence band, but the upper boundary diverged giving no upper limit to the confidence band.

The observed increase in particle fluorescence was unexpected, and suggests a significant shift in the local environment of the fluorophore on the apoE protein (e.g. polarity) or a substantial protein conformational shift impacting the distance between fluorophore molecules. Importantly, this effect is seen only in media, and only in NLPs with lipids in the gel phase at 37°C (*vide infra*). While this is reproducibly observed in only two NLP formulations in media, additional studies are merited to understand this phenomenon.

In addition to acyl chain length, double bonds are another structural feature in the acyl chain that influence the properties of lipids and their bilayer. Cis double bonds in the acyl chain are known

to decrease bilayer viscosity and lower liquid-gel phase transition temperatures relative to saturated lipids of the same length.[23] Comparing NLPs prepared with saturated or unsaturated lipid acyl chains of the same carbon chain length (e.g. 18:0 versus 18:1) demonstrates that saturated species was substantially more stable in media, exhibiting increased $t_{1/2}$ values relative to NLPs with the corresponding unsaturated species ($t_{1/2}$ = 82 and 10.4 hrs, respectively) (Table 1). This observation was mirrored with NLPs prepared with the lipids featuring acyl chains with two double bonds (18:2) (Fig. 2h), which were found to be considerably less stable in media than 18:1 NLPs (Fig. 2b) ($t_{1/2}$ = 1 hr and 10.4 hrs, respectively). These results indicate that NLP stability in media, as measured by the $t_{1/2}$, is directly correlated with chain length yet inversely correlated to the number of cis double bonds for a given acyl chain. Interestingly, NLPs prepared with 1-palmitoyl-2-oleoyl-sn-glycero-3-phosphocholine (POPC), comprised of two acyl chains of different length and saturation (16:0 and 18:1) (Fig. 2i, $t_{1/2}$ = 5 hours), were less stable than either 16:0 or 18:1 NLPs (where both acyl chains were identical) ($t_{1/2}$ = 61 and 10.4 hours, respectively).

As an additional comparison, NLPs were prepared with 18:1 lipids possessing trans, rather than cis, double bonds (denoted as 18:1t). This lipid is an isomer of DOPC (18:1 cis), wherein the acyl chain with the double bond is oriented vertically rather than bending out from the vertical axis of the lipid, leading to a stiffer bilayer.[24] We hypothesized that these NLPs would exhibit enhanced stability stable in serum solutions relative to DOPC, mirroring the results observed with the more compact saturated lipid bilayers. Surprisingly, these NLPs exhibited a $t_{1/2}$ of 4.9 (Fig. 2j) hours, significantly lower than the 10.4 hours determined for 18:1 cis. The exact cause of this difference is unclear, but implies that lipid bilayer stiffness is not the sole (or predominant) predictor of NLP stability. Other stabilizing forces, including lipid-apolipoprotein interactions, could contribute to the stability differences between formulations with 18:1 cis and 18:1 trans. All of the $t_{1/2}$ results are summarized in Fig. 2k.

Effect of lipid chain length and saturation on NLP stability in neat serum

Fetal bovine serum (FBS) is an excellent *ex vivo* surrogate for simulating the *in vivo* biological aqueous milieu that NLPs would encounter when systemically administered into the bloodstream. While compositionally similar to plasma (i.e. cell-free), serum is purified from

whole blood after coagulation has occurred. The total protein concentration in serum (e.g. FBS) exceeds 53 mg/mL, dominated primarily by albumin and globulins. A number of serum components are known to directly interact with HDLs and would hence impact particle stability, in particular endogenous apolipoproteins (such as apoA-I) which are present in serum at concentrations up to 10 mg/ml.[25,26] Synthetic lipoproteins are known to interact with endogenous lipoproteins to dynamically exchange constituents, including apoliporoteins and lipids.[8,27] It is worth noting that frozen, purified HDLs have been shown to have reduced activity,[28] but it is unclear if the same is true for HDLs frozen in whole serum (as used in this study), and whether this could alter the interactions between our particles and serum components. Additionally, lecithin:cholesterol acyltransferase (LCAT) is also present in serum and is known to bind to HDLs.[29] LCAT enzymatic activity, which involves producing lysophospholipids and cholesterol esters, is known to be activated by ApoE and causes remodeling of rHDLs,[30] though it is unclear what effect it would have on particles lacking cholesterol. Thus, it is readily expected that incubating NLPs in neat serum, with the undiluted serum comprising more than 90% of the solution volume, results in NLP dissociation much more rapidly than in media supplemented with 10% serum.[15] However, a thorough quantification of the differential stability of NLPs prepared with various lipids provides valuable insight into both structure-function relationships between the scaffold and lipid bilayer, and ultimately impacts design considerations for NLP formulations destined for *in vivo* applications.

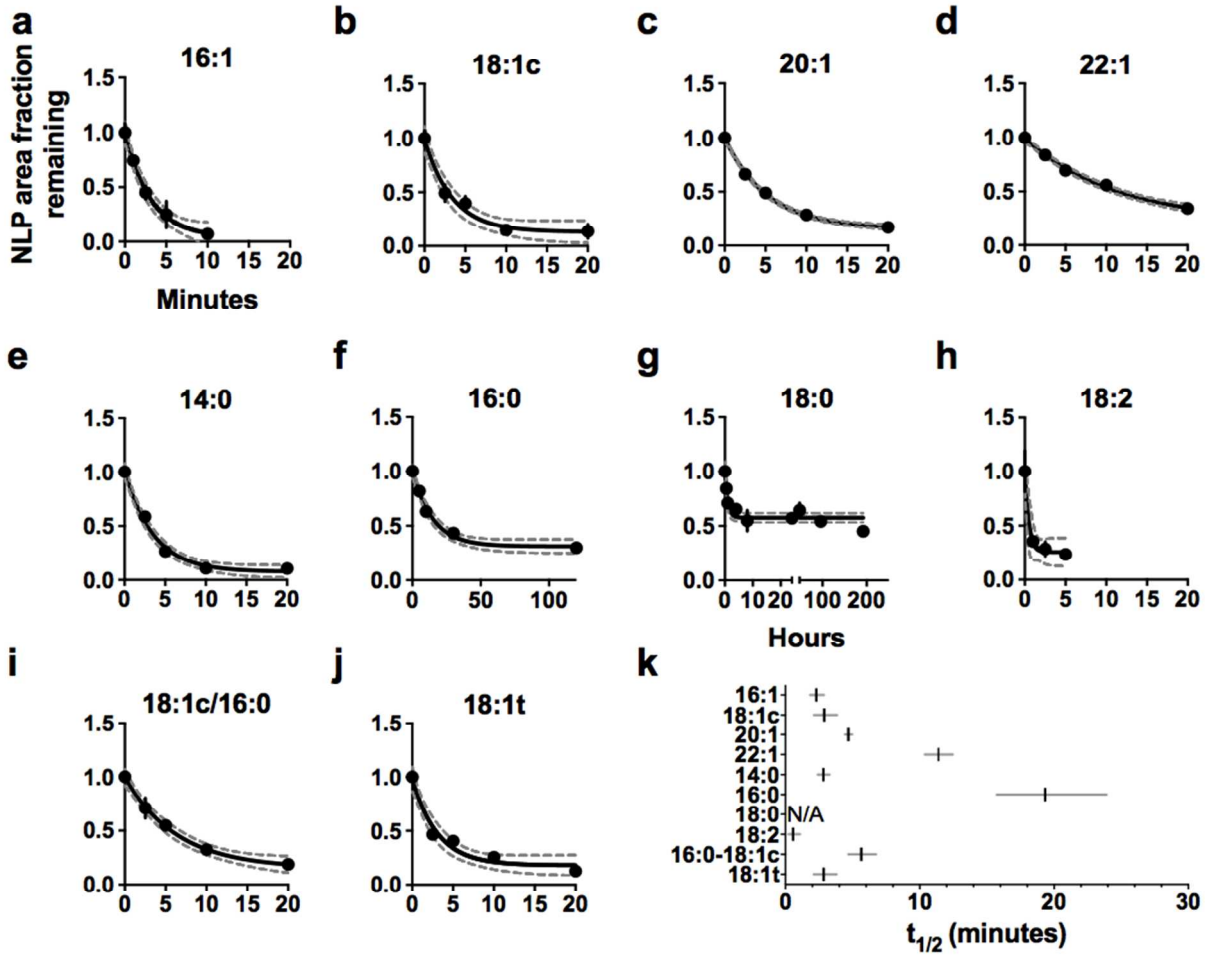

Fig. 3. Charaterization of NLP stability in neat fetal bovine serum, measuring the change in NLP peak area fraction over time at 37°C. (a-j) Individual stability assessments, whereby X- and Y-axes are represented as the NLP area fraction remaining relative to t=0 and incubation time in minutes (a-f, h-j) or hours (g), respectively. The coefficient of determination (R^2) is listed for each fitted regression fit. (a) 16:1 NLP, $R^2 = 0.97$. (b) 18:1 NLP, $R^2 = 0.96$. (c) 20:1 NLP peak, $R^2 = 1.0$. (d) 22:1 NLP, $R^2 = 0.99$. (e) 14:0 NLP, $R^2 = 0.99$. (f) 16:0 NLP, $R^2 = 0.98$. (g) 18:0 NLP, $R^2 = 0.87$. Note discontinuous x-axis. (h) 18:2 NLP, $R^2 = 0.94$. (i) 16:0-18:1 cis NLP, $R^2 = 0.98$. (j) 18:1 trans NLP, $R^2 = 0.96$. (k) Summary graph of $t_{1/2}$ values.

High serum concentrations significantly decreased NLP stability, as $t_{1/2}$ values were measured on the order of minutes rather than hours (Fig. 3). However, the trends between the different lipid types closely mirror what was observed in media supplemented with 10% serum. For example, NLPs incorporating lipids with longer mono-unsaturated chains exhibited longer $t_{1/2}$ times. The 16:1 and 18:1 NLPs (Fig. 3a and 3b) exhibited similar stabilities, with overlapping 95% confidence intervals. As anticipated, the 20:1 (Fig. 3c) and 22:1 (Fig. 3d) NLPs were more stable, but still exhibited $t_{1/2}$ values less than 12 minutes (Table 1).

Table 1: NLP stabiliy values in media and serum

	Media (hours)				FBS (minutes)			
Lipid	$t_{1/2}$ Lower limit	$t_{1/2}$	$t_{1/2}$ Upper limit	k_{decay}	$t_{1/2}$ Lower limit	$t_{1/2}$	$t_{1/2}$ Upper limit	k_{decay}
16:1	0.4	0.5	0.5	1.765	1.8	2.3	2.9	0.32
18:1c	7.8	10.4	13.8	0.091	2.1	2.9	3.8	0.293
20:1	17.7	21.9	27.1	0.059	4.4	4.7	5	0.19
22:1	None	None	None	0.055	10.4	11.4	12.5	0.089
14:0	0.5	1.1	2	1.33	2.4	2.8	3.3	0.282
16:0	32.5	46.1	25.2	N/A	15.7	19.3	23.9	0.067
18:0	64	82	None	N/A	None	None	None	0.017
18:2	0.5	1	1.7	1.316	0.2	0.6	1.1	1.989
16:0-18:1c	3.6	4.2	5	0.29	4.7	5.6	6.7	0.157
18:1t	3.8	4.9	5.9	0.248	2.1	2.8	3.8	0.323
24:1					9.3	12.2	15.7	0.115

Among the lipids with saturated chains, the 14:0 NLPs (Fig. 3e) had the shortest $t_{1/2}$, and were comparable to 18:1 NLPs ($t_{1/2}$ = 2.8 and 2.9 min, respectively). The 16:0 NLPs (Fig. 3f) had a longer $t_{1/2}$ time (19.3 min) than the 14:0 lipid as well as all of the lipids with unsaturated chains. Perhaps the most interesting result is the 18:0 NLP (Fig. 3g), which exhibited a plateau in its decay curve above 50% of the initial NLP area. This plateau persisted as long as 8 days in the FBS solution. To confirm that these were particles capable of complete dissociation, the 18:0 NLPs were incubated in PBS with 250 mM sodium cholate at 100°C to fully disrupt the particle and denature the protein, and then analyzed by aSEC (Fig. S3). These conditions successfully released the scaffold protein from the NLP, suggesting that indeed this formulation exhibits exceptional stability in FBS at 37°C.

Mirroring the results in media, the 18:2 NLP (Fig. 3h) possessed the shortest $t_{1/2}$ in serum, dissociating to half of the initial area within the first minute of exposure to serum. Surprisingly,

the 16:0-18:1 cis (POPC) formulation (Fig. 3i) had a $t_{1/2}$ that was greater than 18:1 cis (DOPC) formulation in these experiments, placing its stability between 18:1 and 16:0 as originally hypothesized. It is unclear why the measured behavior is different in serum compared to media. NLPs prepared with either cis or trans version (Fig. 3j) of 18:1 exhibited similar $t_{1/2}$ (12.8 and 12.9 min, respectively). All of the serum stability results are summarized in Fig. 3k.

Overall, these results show that NLPs dissociate far more readily in serum solutions than in media. With the exception of the relative differences in behavior of the 16:0-18:1 cis (POPC) and 18:1 trans formulations, similar trends between acyl chain structure and $t_{1/2}$ value were observed, with all but one formulation exhibiting a $t_{1/2}$ under 20 minutes. The 18:0 NLP was notable in this regard, as less than 50% of the NLP peak was lost during the first 4 days of incubation, though by the day 8, only 45% of the peak area was remaining. While we have reported on NLP formulations containing crosslinked lipids that are extremely stable in serum in the past,[22] this formulation represents a possible alternative for *in vivo* applications without the need for the addition of crosslinking lipids.

Distinct trends are observed in stability of NLPs with mono-unsaturated and saturated lipids of increasing acyl chain length (Fig. 4). While we were not able to correlate these results with chain length independent of degree of unsaturation, we were able to find linear correlations between chain length and $t_{1/2}$ values for lipids with the same degree of saturation. In both media (Fig. 4a) and serum (Fig. 4b), longer chain length provides enhanced stability within each lipid class. For the results of particles in media, the saturated series had an $R^2 = 0.98$. and the mono-unsaturated series had an $R^2 = 1.0$. In serum, the mono-unsaturated series followed an exponential fit ($R^2 = 0.968$). Based on the trend observed with the mono-unsaturated series in media with carbon lengths ranging from 16 – 22 (Fig. 4b), one would expect that NLPs with longer acyl chains (i.e. 24:1 NLPs) would exhibit enhanced stability. However, the experimental $t_{1/2}$ was significantly lower than the predicted value for the 24:1 NLPs ($t_{1/2}$ = 12 vs. 22 minutes, respectively) (Fig. S4). This suggests that while increasing chain length tracks with an increase in NLP $t_{1/2}$, there may be physical limits to this trend with lipids exceeding 22 carbon atoms, though additional experiments are needed to confirm this. It is important to note that lipids with acyl chains with 22 or more carbons and a single double bond are exceedingly rare in mammalian tissues.[31]

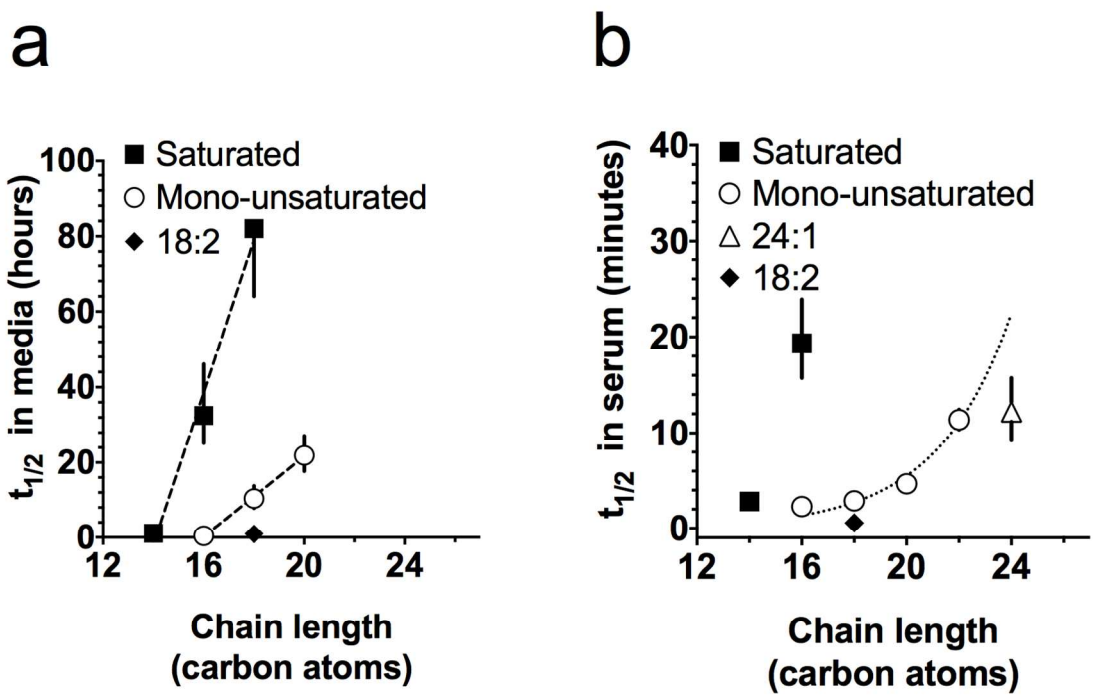

Fig. 4. Comparisons of stability as a function of lipid acyl chain length in (a) media and (b) serum (saturated R^2 = 0.98, mono-unsaturated R^2 = 1.0). The $t_{1/2}$ of mono-unsaturated lipid formualtions in serum fit a regression model (R^2 = 0.97).

As chain length alone was not an accurate deterimant of NLP stability, we investigated other particle and lipid bilayer characteristics for direct correlations with the rate of NLP dissociation. We plotted the $t_{1/2}$ versus the initial particle size, but found no substantial correlation(R^2 = 0.35, Fig. S5). While key parameters for many of these lipids have been independently reported in the literature, values easily differ up to 30% between studies, potentially confounding any correlation between lipid characteristics and $t_{1/2}$ values in this study. In order to ensure consistency, key intrinsic lipid parameters for the lipids in this study were calculated at 37°C using all-atom MD simulations of solvated lipid bilayers. Computed parameters included area-per-lipid, water penetration into the acyl chain region, bilayer thickness, and the bilayer area compressibility modulus (K_A). Representative snapshots of the simulation for 18:1, 14:0, and

18:0 bilayers are provided in Fig. 5a-c. All computed averages and standard errors are listed in Table 2. As expected, 16:0 and 18:0 were the only lipid bilayers not in a liquid phase at 37°C. [32] Confinement of lipids in rHDLs has been shown to shift the liquid to gel phase transition temperature a few degrees higher, at 37°C this would not affect the phase of the lipids studied here. [33] Under these conditions, 16:0 is in the gel phase and 18:0 in a tilted gel phase. For 18:0, the simulated values for area per lipid (50.8 Å) and lipid tilt (approximately 37° from the bilayer normal) mirrored both previous reported experimental (area of 52.0 $Å^2$ and tilt of 38°)[34] and simulation work (area of 50.2 $Å^2$ and tilt of 37.5°).[35]

Table 2: Computed lipid parameters using all-atom molecular simulation at 37°C

Lipid tail structure	Area per lipid ($Å^2$) (± std. error)	Water penetration (±std. error)	Bilayer thickness (P-P distance, Å) (±std. error)	Compressibility modulus (K_A, mN/m) (±std. error)
16:1	68.4 (±0.8)	3.45 (±0.10)	35.3 (±0.3)	285.2 (±34.8)
18:1c	68.7 (±0.9)	3.53 (±0.10)	38.4 (±0.4)	252.3 (±16.9)
20:1	66.9 (±0.8)	3.30 (±0.10)	42.5 (±0.4)	300.3 (±49.8)
22:1	65.3 (±0.8)	3.19 (±0.09)	46.8 (±0.5)	317.6 (±27.5)
14:0	60.2 (±0.9)	2.89 (±0.12)	36.0 (±0.4)	229.8 (±58.9)
16:0	50.3 (±0.6)	1.77 (±0.10)	43.3 (±0.3)	476.2 (±146.2)
18:0	50.8 (±0.3)	1.71 (±0.11)	46.2 (±0.2)	1764.9 (±157.4)
18:2	70.4 (±0.9)	3.61 (±0.10)	37.0 (±0.4)	275.1 (±20.6)
16:0-18:1c	64.6 (±0.8)	3.20 (±0.10)	38.9 (±0.4)	272.0 (±17.8)
18:1t	Not determined	Not determined	Not determined	Not determined
24:1	62.9 (±0.8)	3.08 (±0.11)	51.7 (±0.5)	307.0 (±68.5)

For the bilayer area area compressibility modulus (K_A) measurements (Fig. 5d), we found that most bilayers had values that ranged from 200-300 mN/m, in very good agreement with the experimental and computational range observed for liquid phases.[36] The gel phase lipids 16:0

and 18:0 exhibited significantly higher area compressibility (476 and 1764 mN/m, respectively). Similarly, these two lipids had the least amount of water penetration into the hydrophobic core of the bilayer (Fig. 5e), as well as the lowest area per lipid, which is consistent with a denser gel phase bilayers. However, the bilayer thicknesses for these two lipids (16:0 = 43 Å, 18:0 = 46 Å) were comparable to the longer chained mono-unsaturated lipids (e.g. 20:1 and 22:1) and less than the 24:1 lipid (52 Å).

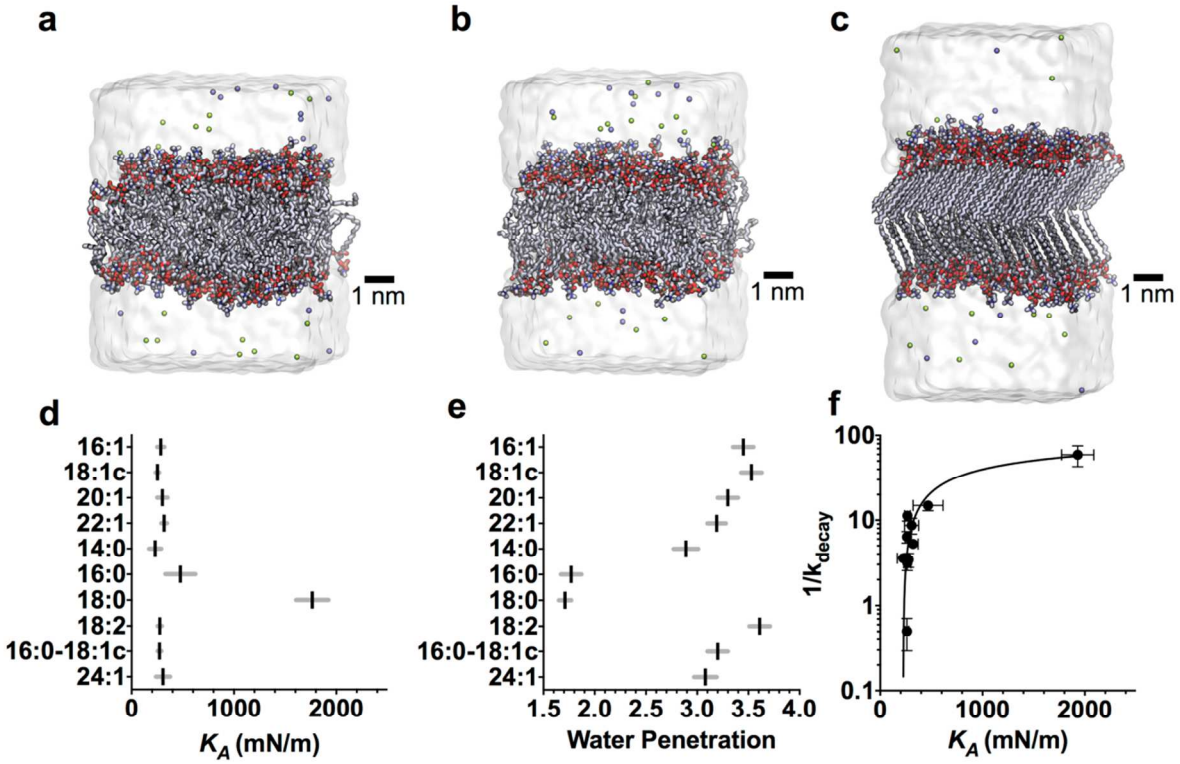

Fig. 5. Correlating computed lipid parameters with NLP stability. (a) Simulation snapshot of the 18:1 cis bilayer (200 ns, liquid phase). (b) Simulation snapshot of the 14:0 bilayer (200 ns, liquid phase). (c) Simulation snapshot of the 18:0 bilayer (200ns, tilted gel phase). (d) Summary plot of K_A values for key lipids used in this study. (e) Summary plot of water penetration into the bilayer core for key lipids used in this study, expressed as molecules of water within 0.4 nm of the hydrophobic core per lipid molecule in the simulation. (f) Analysis of the inverse of the experimentally-derived NLP decay constant as a function of the computed bilayer compressibility modulus (K_A, R^2 = 0.95).

The gel-phase lipids, 16:0 and 18:0, were distinct outliers relative to the other lipids in terms of area-per-lipid, water penetration, and compressibility modulus (Table 2). The correlations between these key parameters and NLP stability were assessed. However, as the $t_{1/2}$ was not readily calculated for the 18:0 lipid due to the plateauing of the dissociation trend, the decay

constant (k_{decay}) for each NLP formulation was calculated. When the inverse of the decay constant was plotted against K_A (Fig. 5f), the data was fit to a natural logarithmic function with an R^2 value of 0.95. Plots correlating water penetration, area-per-lipid, or bilayer thickness with the inverse of the decay constant failed to show highly significant trends (Fig. S6).

The apparent relationship between the decay constant and K_A suggests that the rate of dissociation of these particles in serum is related to the compressibility (or elasticity) of the bilayer component of these particles. In other words, the NLP stability is related to the force required to laterally stretch the lipid bilayer. The correlation between dissociation rate and elasticity suggests that NLPs more susceptible to deformation (due to a decrease in compressibility modulus) are less stable in a complex biological milieu. The exact mechanism by which this occurs, and which serum components may play a key role in the NLP dissociation, are currently unknown. However, these results provide a novel insight into aspects of the NLP bilayer that are key determinants in this process. While the interplay between bilayer elasticity and lipid molecular structure has been well studied in larger lipidic structures (e.g. giant unilamellar vesicles),[24] the current study represents novel insight into the role of bilayer elasticity as one of the factors in stabilizing structures below 20 nm in diameter, as well as in lipidic structures supported and stabilized by protein components (i.e. apolipoproteins). Interestingly, as discussed above, NLPs prepared with these two gel-phase lipids also exhibited anomalous dissociation profiles in media (Figure 2f and 2g). These combined data and observations suggest that the NLP bilayer, and the lipid:apolipoprotein interactions, are in some ways unique, and merit additional study to elicudiate the potential structure and mechanism of association.

Based on our results, the NLP dissociation process can be predicted based on a universal lipid bilayer elastic property. However, it is important to note that the extent to which elasticity determines the rate of dissociation may vary between rHDL formulations prepared with different apolipoproteins. First, NLP apolipoprotein constituents may interact differently with serum components. Second, the size of the NLP, dictated by both apolipoprotein and lipid constituents, can also play an important role in bilayer characteristics and serum interactions. Third, the interaction between the apolipoprotein and lipid bilayer can significantly vary depending on acyl chain structure and bilayer thickness, and merits further study.

While much of the discussion has focused on the process through which the NLPs dissociate, the ultimate fate of the NLPs themselves is also of interest. Our initial hypothesis was that all NLP formulations would fully dissociate over time, and the NLP peak area would approach 0% of the initial area (as observed in Fig. 3e for 14:0). Unexpectedly, non-zero plateaus were observed for a number of NLP formulations in both media and serum, with $t_{1/2}$ values up to 0.58 for 18:0 NLPs. While there was only weak correlation between dissociation plateau values with the K_A (R^2 = 0.76) (Fig. S7), we hypothesize that other bilayer parameters, such as the bilayer bending modulus or lipid spontaneous curvature, could have a better correlation to the plateau values. Interestingly, a linear relationship was observed in both saturated and mono-unsaturated NLP formulations (R^2 of 0.92 and 0.96, respectively) when bilayer thickness was plotted against the dissociation plateau values (Fig. 6a).

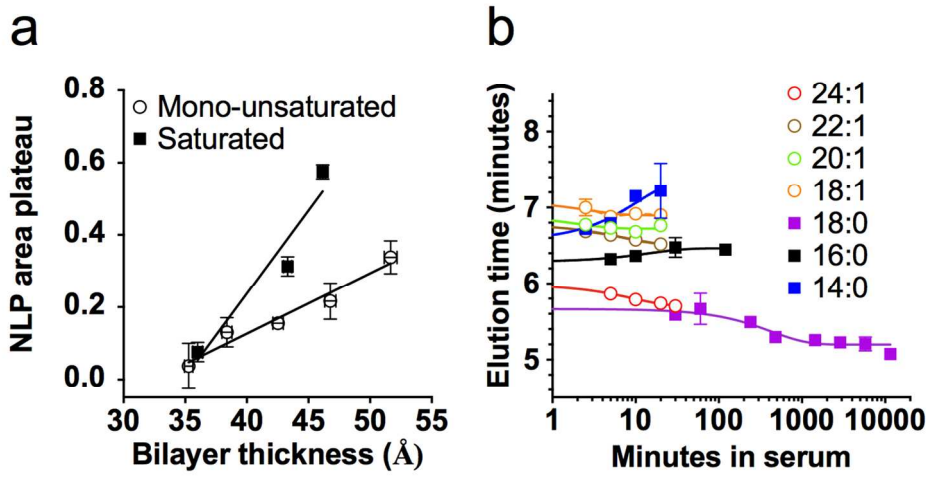

Fig. 6. (a) NLP area plateau versus computed bilayer thickness, saturated R^2 = 0.92, mono-unsaturated R^2 = 0.96. (b) a plot showing the NLP peak center changing over time due to incubation in serum.

While assessing the composition of NLPs following serum incubation was outside the scope of this study, it was observed that the NLP retention time shifted over time (represented in Fig. 1b). We initially expected a gradual increase in NLP size, coinciding with the well-documented formation of a protein corona.[37,38] or remodeling of the NLPs into larger LDL- or VLDL-like structures. This could occur as a result of endogenous apolipoproteins associating with the

particles, and the particles that comprise the plateau at longer time points could consist of mixtures of the NLP scaffold and endogenous apolipoproteins. However, while NLPs with mono-unsaturated lipids increased in size over time (indicated by progressively shorter retention times), NLPs with saturated lipids exhibited variable size changes over time (Fig. 6b). In particular, both 14:0 and 16:0 NLPs decrease in size over time. In contrast, 18:0 NLPs continuously increased in size over time, maintaining structural integrity (with no visible aggregation) over 8 days. Using protein reference standards, we estimate the size of these particles to be at least 800 kDa. The two distinct trends in NLP size change over time suggest there are multiple mechanisms by which NLPs dissociate in serum, and merits further in depth analysis to elucidate these processes. We hypothesize that the interaction between apolipoprotein and the lipid bilayer is substantially different depending on the acyl chain composition of the bilayer lipid, especially for lipids in the gel phase such as 18:0. A systematic analysis of NLP composition (e.g. apolipoprotein-to-lipid ratio and apolipoprotein type) and size would provide additional insights into the mechanism of dissociation under physiological conditions, as these factors also contribute significantly to NLP stability. To that end, using dual labeled, fluorescent NLPs to simultaneously track protein and lipid constituents is could help elucidate the mechanism of dissociation. [39]

Conclusions

The stability of synthetic HDLs has important implications for the myriad biological applications of these versatile nanoparticles. While others have characterized stability of lipidic structures under various non-physiological conditions,[18,40] this study constitutes the first systematic stability assessment of a wide range of NLPs in conditions encountered under biologically-relevant *in vitro* and *in vivo* conditions. We found that NLPs prepared with phosphatidylcholine lipids readily dissociate over time in fetal bovine serum, and that the rate of dissociation is related to serum concentration. However, this dissociation rate is significantly impacted by the acyl chain structure of the lipid comprising the homogeneous lipid bilayer, spanning two orders of magnitude in neat serum. The key lipid parameter that correlated with NLP stability is the compressibility modulus (K_A) of the lipid bilayer, exhibiting an inverse relationship with the rate of dissociation of the particles (k_{decay}), meaning that NLPs featuring bilayers with higher compressibility moduli dissociate slower in serum. Interestingly, not all formulations fully

dissociate in serum over relevant timescales, suggesting that some NLP composition may be more resistant to dynamic rearrangement with endogenous lipoproteins or other serum constituents. These findings provide a novel insight into tunable nature of synthetic HDLs, and can be used to optimize particle characteristics for specific in vivo therapeutic or diagnostic applications.

Materials and Methods

Materials

1,2-dilinoleoyl-sn-glycero-3-phosphocholine (14:1), 1,2-dipalmitoleoyl-sn-glycero-3-phosphocholine (16:1), 1,2-dioleoyl-*sn*-glycero-3-phosphocholine (DOPC/18:1 cis), 1,2-dielaidoyl-sn-glycero-3-phosphocholine (18:1 trans), 1,2-dieicosenoyl-sn-glycero-3-phosphocholine (20:1), 1,2-dierucoyl-sn-glycero-3-phosphocholine (22:1), 1,2-dinervonoyl-sn-glycero-3-phosphocholine (24:1), 1,2-dimyristoyl-*sn*-glycero-3-phosphocholine (DMPC/14:0), 1,2-dipalmitoyl-sn-glycero-3-phosphocholine (DPPC/16:0), 1,2-distearoyl-sn-glycero-3-phosphocholine (DSPC/18:0), 1,2-dilinoleoyl-sn-glycero-3-phosphocholine (18:2), and 1-palmitoyl-2-oleoyl-sn-glycero-3-phosphocholine (POPC/16:0-18:1 cis) were purchased from Avanti Polar Lipids (Alabaster, AL). All other reagents were ordered from Sigma-Aldrich (St. Louis, MO). RPMI-1640 cell culture media was purchased from ATCC (Manassas, VA). Fetal bovine serum, Penicillin/Streptomycin, and Alexa Fluor 488 NHS Ester (AF488) were obtained from Invitrogen (Carlsbad, CA).

Protein expression and purification

The expression clone for the 22 kDa N-terminal fragment of human apolipoprotein E4 (apoE422k, kindly provided by Dr. Karl Weisgraber) featuring a cleavable His-tag[41] was expressed and purified as previously described.[15,42]

NLP assemblies

NLPs were assembled according to a previously reported procedure[5,43] with slight modifications. Assembling NLPs with a certain lipid type and scaffold protein can produce a number of different NLP species, but their homogeneity and stability can be highly variable.[44] For each new lipid or lipid mixture, assembly ratios were empirically derived to produce particles with greatest homogeneity and to minimize excess protein following the reaction. These ratios are given in Table 3 below. Briefly, lipids were either prepared or obtained in chloroform and aliquoted into glass vials. Chloroform was then removed using a stream of N_2 under agitation to form a thin lipid film. Lipids were solubilized in PBS buffer (137 mM sodium chloride, 2.7 mM potassium chloride, 10 mM phosphate buffer, pH 7.4) using 80 mM sodium cholate. After addition of the ApoE422k (150 μM in final assembly volume), samples were incubated at 22°C for at least 1 hour. Assemblies were dialyzed overnight against PBS to remove cholate.

Table 3: NLP assembly conditions

Lipid	Lipid:Protein	Reaction temperature
16:1	120:1	25°C
18:1 cis (DOPC)	80:1	25°C
20:1	80:1	25°C
22:1	80:1	25°C
18:1 trans	80:1	25°C
14:0	200:1	25°C
16:0 (DPPC)	160:1	37°C
18:0 (DSPC)	120:1	50°C
18:2	80:1	25°C
16:0-18:1 cis (POPC)	80:1	25°C
24:1	60:1	25°C

Labeling the NLPs with Alexa Fluor dyes

NLPs were labeled with either AF488 by incubating the NLPs with the reactive dye for at least 2 hrs (5:1 dye:NLP molar ratio). The reaction was performed in PBS buffer containing 5 mM sodium bicarbonate, pH 8.2. After completion of the reaction, 10 mM Tris pH 8.0 was added to quench any unreacted dye and incubated for 30 minutes. Free dye in the NLP solution was removed by using a dye-removal column kit, as directed (Thermo Fisher, Rockford, IL).

NLP Purification

Samples were purified by SEC (Superdex 200, 10/300 GL column, GE Healthcare, Piscataway, NJ) in PBS buffer (1.0 mL/min flow rate). The exclusion limit of the column was determined with Blue Dextran 2000. SEC fractions (500 µl) were collected every 60 s. SEC fractions containing homogeneous NLP populations were concentrated using 50 kDa MWCO spin concentrators (Sartorius). A concentration for NLPs in solution was determined by using a Nanodrop ND-1000 spectrophotometer (ThermoScientific, Lafayette, CO) at an absorbance of 280 nm. The concentrated NLP samples were then stored at 4˚C until further use.

SEC analysis of NLP stability in complex biological fluids

NLP samples were incubated in RPMI-1640 with 0.1% Penicillin/Streptomycin and 10% FBS, or neat FBS and subsequently analyzed by analytical SEC (aSEC) (Superdex 200 Increase 3.2/300 column, GE Healthcare) in PBS buffer. A flow rate of 0.2 ml/min was used to ensure minimal overlap in the elution of dissociated apoE422k and intact NLP. Data on elution of reference standards using these conditions is available in Fig. S8. These standards were detected using an SPD-10Ai UV-vis detector (Shimadzu), and elution times were normalized to account for volume delay to the RF-20 fluorescence detector (Shimadzu).

The NLPs labeled with AF488 were monitored using a fluorescence detector set to excite at 495 nm and to measure fluorescence at 520 nm to avoid interfering absorbance from serum proteins and constituents. The raw chromatograph obtained from the fluorescence detector was further analyzed by fitting a series of Gaussian functions to the trace through code written in Python using the lmfit library. Peaks centered between 5 and 8 minutes were considered to be NLP

populations, while free ApoE422k was found to elute at approximately 9.5 minutes under these conditions. The NLP Gaussian functions were then integrated to assess NLP disassembly as a function of time. These peak areas, from independent samples incubated in media or serum for varying times, were then arranged into a time series, and exponential decay functions were fit to each combination of peak areas. For each fit, the function was normalized around time zero, and the half-life of the function was recorded.

Molecular Dynamics (MD) simulations

The bilayer properties of the different lipid types used for exploring NLPs stability were characterized using MD simulations. All the simulations were generated using the CHARMM-GUI *Membrane Builder,*[45,46] and performed using the GROMACS molecular dynamics suite version 5.1.x.[47,48] Each bilayer system contained 144 lipids (72 in each leaflet), 60 water molecules per lipid, and 150 mM NaCl. The CHARMM36 lipid force field[49] was used with the TIP3P water model.[50,51] The initial energy minimization and six-step equilibration was done according to the CHARMM-GUI GROMACS equilibration scripts. Production runs were 200 ns long at 310 K and 1 bar. Temperature was controlled with a Nosé-Hoover thermostat[52] (with a time constant of 1 ps) and pressure with a semi-isotropic Parrinello-Rahman barostat (with a time constant of 5 ps and a compressibility of 4.5×10^{-5} bar^{-1}).[53] The simulations were run under periodic boundary conditions (PBC), time step was 2 fs, the LINCS algorithm[54] was used to restrain h-bonds, Lennard–Jones interactions were cutoff using a force-switch over 1.0 to 1.2 nm, electrostatic interactions were cutoff at 1.2 nm and long-range electrostatic handled with the particle mesh Ewald (PME) method.[55]

For analysis, averages over the last 100 ns of each simulation were used and SE estimated between the last four, 25 ns, segments. The analysis was carried out using GROMACS tools and custom tools written in Python and using the MDAnalysis package.[56,57] The area per lipid was estimated as the box area (along the bilayer plain) divided by the number of lipids per monolayer. The bilayer thickness was defined as the average phosphate distance between the bilayer leaflets. The bilayer area compressibility (K_A) was calculated from the amplitude of the box area fluctuations $K_A = k_B T\langle A\rangle / N\langle (A - A_0)^2\rangle$, where k_B is the Boltzmann constant, T is the absolute temperature in Kelvin, N is the number of lipids in each monolayer, and A_0 is the equilibrium area. The bilayer water access was quantified as average number of water oxygen

atoms within 0.4 nm of the bilayer hydrophobic core (defined as the fatty acid carbon atoms). Simulation snapshots were rendered in Visual Molecular Dynamics (VMD).[58]

Acknowledgements

This work was performed under the auspices of the U.S. Department of Energy under contract number DE-AC52-07NA27344, and was supported by Lawrence Livermore National Laboratory LDRD research awards 15-LW-023 and 17-LW-051.

Supporting Information. 1, SEC traces of purified NLPs used in this study. **2**, the full SEC fluorescence chromatogram for the data shown in Figure 1b and a bar graph showing the total fluorescence area of the curves in S2a. **3**, SEC traces of dissociated DSPC NLPs. **4**, change in NLP fraction over time for 24:1 NLPs in serum. **5**, plot of NLP $t_{½}$ in serum versus the initial NLP peak center in serum. **6**, plots showing $1/K_{decay}$ plotted against the calculated values for water penetration, area per lipid, and bilayer thickness. **7**, plot of NLP area plateau versus elastic modulus. **8**, SEC traces for protein standards run using the same conditions as those used to analyze NLPs in serum solutions.

References

1 J. B. Simonsen, *Nanomed.*, 2016, **12**, 2161–2179.
2 H. Huang, W. Cruz, J. Chen and G. Zheng, *Wiley Interdiscip. Rev. Nanomed. Nanobiotechnol.*, 2015, **7**, 298–314.
3 C. Zhu and Y. Xia, *Chem. Soc. Rev.*, 2017, **46**, 7668–7682.
4 D. A. Bricarello, J. T. Smilowitz, A. M. Zivkovic, J. B. German and A. N. Parikh, *ACS Nano*, 2011, **5**, 42–57.
5 C. D. Blanchette, R. Law, W. H. Benner, J. B. Pesavento, J. A. Cappuccio, V. Walsworth, E. A. Kuhn, M. Corzett, B. A. Chromy, B. W. Segelke, M. A. Coleman, G. Bench, P. D. Hoeprich and T. A. Sulchek, *J. Lipid Res.*, 2008, **49**, 1420–1430.
6 J. P. Segrest, L. Li, G. M. Anantharamaiah, S. C. Harvey, K. N. Liadaki and V. Zannis, *Curr. Opin. Lipidol.*, 2000, **11**, 105–115.
7 Y. Zhao, A. S. Black, D. J. Bonnet, B. E. Maryanoff, L. K. Curtiss, L. J. Leman and M. R. Ghadiri, *J. Lipid Res.*, 2014, **55**, 2053–2063.
8 Y. Zhao, T. Imura, L. J. Leman, L. K. Curtiss, B. E. Maryanoff and M. R. Ghadiri, *J. Am. Chem. Soc.*, 2013, **135**, 13414–13424.
9 B. J. Van Lenten, A. C. Wagner, G. M. Anantharamaiah, M. Navab, S. T. Reddy, G. M.

Buga and A. M. Fogelman, *Curr. Atheroscler. Rep.*, 2009, **11**, 52–57.
10 I. G. Denisov and S. G. Sligar, *Chem. Rev.*, 2017, **117**, 4669–4713.
11 D. Weilhammer, A. D. Dunkle, C. D. Blanchette, N. O. Fischer, M. Corzett, D. Lehmann, T. Boone, P. Hoeprich, A. Driks and A. Rasley, *Vaccine*, 2017, **35**, 1475–1481.
12 N. O. Fischer, E. Infante, T. Ishikawa, C. D. Blanchette, N. Bourne, P. D. Hoeprich and P. W. Mason, *Bioconjug Chem*, , DOI:10.1021/bc100083d.
13 N. O. Fischer, A. Rasley, M. Corzett, M. H. Hwang, P. D. Hoeprich and C. D. Blanchette, *J. Am. Chem. Soc.*, 2013, **135**, 2044–2047.
14 D. R. Weilhammer, C. D. Blanchette, N. O. Fischer, S. Alam, G. G. Loots, M. Corzett, C. Thomas, C. Lychak, A. D. Dunkle, J. J. Ruitenberg, S. A. Ghanekar, A. J. Sant and A. Rasley, *Biomaterials*, 2013, **34**, 10305–10318.
15 N. O. Fischer, D. R. Weilhammer, A. Dunkle, C. Thomas, M. Hwang, M. Corzett, C. Lychak, W. Mayer, S. Urbin, N. Collette, J. Chiun Chang, G. G. Loots, A. Rasley and C. D. Blanchette, *PLoS ONE*, 2014, **9**, e93342.
16 S. Jayaraman, S. Benjwal, D. L. Gantz and O. Gursky, *J. Lipid Res.*, 2010, **51**, 324–333.
17 M. Wadsäter, M. Cárdenas, S. Harloff-Helleberg, S. Maric, N. Skar-Gislinge, S. Midtgaard, L. Arleth, K. Mortensen, R. O. Ryan and J. Simonsen, *Biophys. J.*, , DOI:10.1016/j.bpj.2011.11.1299.
18 M. Guha, D. L. Gantz and O. Gursky, *J. Lipid Res.*, 2008, **49**, 1752–1761.
19 S. Eisenberg, H. G. Windmueller and R. I. Levy, *J. Lipid Res.*, 1973, **14**, 446–458.
20 W. H. Daerr, W. Pethke, E. T. E. Windler and H. Greten, *Biochim. Biophys. Acta BBA - Lipids Lipid Metab.*, 1990, **1043**, 311–317.
21 Z. Zhang, J. Chen, L. Ding, H. Jin, J. F. Lovell, I. R. Corbin, W. Cao, P.-C. Lo, M. Yang, M.-S. Tsao, Q. Luo and G. Zheng, *Small*, 2010, **6**, 430–437.
22 S. F. Gilmore, C. D. Blanchette, T. M. Scharadin, G. L. Hura, A. Rasley, M. Corzett, C. Pan, N. O. Fischer and P. T. Henderson, *ACS Appl. Mater. Interfaces*, 2016, **8**, 20549–20557.
23 B. R. Lentz, Y. Barenholz and T. E. Thompson, *Biochemistry (Mosc.)*, 1976, **15**, 4529–4537.
24 W. Rawicz, K. C. Olbrich, T. McIntosh, D. Needham and E. Evans, *Biophys. J.*, 2000, **79**, 328–339.
25 X. Zheng, H. Baker, W. S. Hancock, F. Fawaz, M. McCaman and E. Pungor, *Biotechnol. Prog.*, 2006, **22**, 1294–1300.
26 G. L. Francis, *Cytotechnology*, 2010, **62**, 1–16.
27 M. Nakano, M. Fukuda, T. Kudo, M. Miyazaki, Y. Wada, N. Matsuzaki, H. Endo and T. Handa, *J. Am. Chem. Soc.*, 2009, **131**, 8308–8312.
28 M. Holzer, S. Kern, M. Trieb, A. Trakaki and G. Marsche, *J. Lipid Res.*, , DOI:10.1194/jlr.D075366.
29 X. Rousset, B. Vaisman, M. Amar, A. A. Sethi and A. T. Remaley, *Curr. Opin. Endocrinol. Diabetes Obes.*, 2009, **16**, 163–171.
30 Y. Zhao, F. E. Thorngate, K. H. Weisgraber, D. L. Williams and J. S. Parks, *Biochemistry (Mosc.)*, 2005, **44**, 1013–1025.
31 L. Hodson, C. M. Skeaff and B. A. Fielding, *Prog. Lipid Res.*, 2008, **47**, 348–380.
32 D. Marsh, *Handbook of Lipid Bilayers*, CRC Press, Boca Raton, second edition., 2013.
33 I. G. Denisov, M. A. McLean, A. W. Shaw, Y. V. Grinkova and S. G. Sligar, *J. Phys. Chem. B*, 2005, **109**, 15580–15588.
34 A. Tardieu, V. Luzzati and F. C. Reman, *J. Mol. Biol.*, 1973, **75**, 711–733.

35 P. S. Coppock and J. T. Kindt, *Langmuir*, 2009, **25**, 352–359.
36 A. S. Reddy, D. T. Warshaviak and M. Chachisvilis, *Biochim. Biophys. Acta BBA - Biomembr.*, 2012, **1818**, 2271–2281.
37 D. Docter, D. Westmeier, M. Markiewicz, S. Stolte, S. K. Knauer and R. H. Stauber, *Chem. Soc. Rev.*, 2015, **44**, 6094–6121.
38 M. Lundqvist, C. Augustsson, M. Lilja, K. Lundkvist, B. Dahlbäck, S. Linse and T. Cedervall, *PLoS ONE*, 2017, **12**, e0175871.
39 Q. Lin, J. Chen, K. K. Ng, W. Cao, Z. Zhang and G. Zheng, *Pharm. Res.*, 2014, **31**, 1438–1449.
40 M. Wadsater, S. Maric, J. B. Simonsen, K. Mortensen and M. Cardenas, *Soft Matter*, 2013, **9**, 2329–2337.
41 P. C. . Rensen, R. L. . de Vrueh, J. Kuiper, M. K. Bijsterbosch, E. A. . Biessen and T. J. . van Berkel, *Lipid Assem. Drug Deliv.*, 2001, **47**, 251–276.
42 B. A. Chromy, E. Arroyo, C. D. Blanchette, G. Bench, H. Benner, J. A. Cappuccio, M. A. Coleman, P. T. Henderson, A. K. Hinz, E. A. Kuhn, J. B. Pesavento, B. W. Segelke, T. A. Sulchek, T. Tarasow, V. L. Walsworth and P. D. Hoeprich, *J. Am. Chem. Soc.*, 2007, **129**, 14348–14354.
43 B. A. Chromy, E. Arroyo, C. D. Blanchette, G. Bench, H. Benner, J. A. Cappuccio, M. A. Coleman, P. T. Henderson, A. K. Hinz, E. A. Kuhn, J. B. Pesavento, B. W. Segelke, T. A. Sulchek, T. Tarasow, V. L. Walsworth and P. D. Hoeprich, *J. Am. Chem. Soc.*, 2007, **129**, 14348–14354.
44 N. O. Fischer, C. D. Blanchette, B. W. Segelke, M. Corzett, B. A. Chromy, E. A. Kuhn, G. Bench and P. D. Hoeprich, *PLoS ONE*, 2010, **5**, e11643.
45 S. Jo, T. Kim, V. G. Iyer and W. Im, *J. Comput. Chem.*, 2008, **29**, 1859–1865.
46 J. Lee, X. Cheng, J. M. Swails, M. S. Yeom, P. K. Eastman, J. A. Lemkul, S. Wei, J. Buckner, J. C. Jeong, Y. Qi, S. Jo, V. S. Pande, D. A. Case, C. L. Brooks, A. D. MacKerell, J. B. Klauda and W. Im, *J. Chem. Theory Comput.*, 2016, **12**, 405–413.
47 S. Pronk, S. Páll, R. Schulz, P. Larsson, P. Bjelkmar, R. Apostolov, M. R. Shirts, J. C. Smith, P. M. Kasson, D. van der Spoel, B. Hess and E. Lindahl, *Bioinformatics*, 2013, **29**, 845–854.
48 M. J. Abraham, T. Murtola, R. Schulz, S. Páll, J. C. Smith, B. Hess and E. Lindahl, *SoftwareX*, 2015, **1–2**, 19–25.
49 J. B. Klauda, R. M. Venable, J. A. Freites, J. W. O'Connor, D. J. Tobias, C. Mondragon-Ramirez, I. Vorobyov, A. D. MacKerell and R. W. Pastor, *J. Phys. Chem. B*, 2010, **114**, 7830–7843.
50 W. L. Jorgensen, J. Chandrasekhar, J. D. Madura, R. W. Impey and M. L. Klein, *J. Chem. Phys.*, 1983, **79**, 926–935.
51 S. R. Durell, B. R. Brooks and A. Ben-Naim, *J. Phys. Chem.*, 1994, **98**, 2198–2202.
52 W. G. Hoover, *Phys. Rev. A*, 1985, **31**, 1695–1697.
53 M. Parrinello and A. Rahman, *J. Appl. Phys.*, 1981, **52**, 7182–7190.
54 B. Hess, H. Bekker, H. J. C. Berendsen and J. G. E. M. Fraaije, *J. Comput. Chem.*, 1997, **18**, 1463–1472.
55 T. Darden, D. York and L. Pedersen, *J. Chem. Phys.*, 1993, **98**, 10089–10092.
56 N. Michaud-Agrawal, E. J. Denning, T. B. Woolf and O. Beckstein, *J. Comput. Chem.*, 2011, **32**, 2319–2327.
57 R. J. Gowers, M. Linke, J. Barnoud, T. J. E. Reddy, M. N. Melo, S. L. Seyler, J.

Domański, D. L. Dotson, S. Buchoux, I. M. Kenney and O. Beckstein, in *Proceedings of the 15th Python in Science Conference*, eds. S. Benthall and S. Rostrup, 2016, pp. 98–105.
58 W. Humphrey, A. Dalke and K. Schulten, *J. Mol. Graph.*, 1996, **14**, 33–38.

Table of Contents Image

Nanolipoprotein assembly, and dissociation through contact with serum, as assessed through size-exclusion chromatography.